Journal of Applied Biomaterials & Biomechanics 2005; Vol. 3 no. 3: 176-183

Study of non stationary mode flow of an abdominal aortic aneurysm

C. GENEVÈS[1], F. WILQUEM[4], F. TREYVE[2,3], G. CLOUTIER[2,3], G. SOULEZ[2,3], K. SAÏDANE[1,2,3]

[1] Département de Génie Mécanique, École Polytechnique de Montréal - Canada
[2] Institut de Génie Biomédical, École Polytechnique de Montréal - Canada
[3] Centre de Recherche du Centre Hospitalier de l'Université de Montréal, Montréal - Canada
[4] Numeca International - Belgium

ABSTRACT: ***Introduction:*** *Abdominal aortic aneurysm rupture is 95% lethal. Numerical simulation of Navier-Stokes equations allows seeing complex flow phenomenon in laminar state.*
Method: *In this study, we work on a model using the finite element method with an actual 3D geometry. This geometry is from a point cloud obtained by a tomodensitometry scan of a typical patient. We consider rigid wall, homogeneous and Newtonian fluid. We impose four pulsative waveforms as entrance condition: two rest waveforms, two exercise waveforms. The four average Reynolds numbers are 353 and 363 for the rest waveforms and 1058 and 1388 for the exercise waveforms. For the systolic peaks, the Reynolds numbers are 1639 and 1917 for the rest waveforms and 2800 and 2497 for the exercise waveforms.*
Results: *Results show that during the systolic acceleration, vortices issued from the previous pulsation are pushed out and the flow reattached on the wall. During the systolic deceleration, a main vortex appears in the upper part of the aneurysm; it grows and moves to the center. During the diastole, the vortex sustains itself until the next pulsation for the exercise conditions. For the rest conditions, imposed oscillations during the diastole lead to secondary vortices. Pressure stays relatively constant in the aneurysm following the entrance conditions.*
Discussion: *These results on the flow and pressure repartition agreed with those found in the literature (1-6) validating in a first time our model. The next step of the study is the wall shear stress data exploitation. (Journal of Applied Biomaterials & Biomechanics 2005; 3: 176-83)*

KEY WORDS: *Numerical modelling, Three-dimensional geometry reconstruction, Human abdominal aortic aneurysm, Pulsate blood flow*

Received 30/06/05; Revised 20/09/05; Accepted 23/09/05

INTRODUCTION

Abdominal aortic aneurysm (AAA) is a cardiovascular disease that occurs in the infrarenal segment of the descending aorta. It is a dilatation of the vessels due to a weakening or stiffening of the wall (7). The AAA rupture is lethal for 95% of cases (8).
Investigations focus on the studies of the wall and the mechanical stress, detailing the effect of the aneurysm geometry, atherosclerosis and thrombus (9, 10). Other studies focus on the hemodynamic through the aneurysm.
Simple models describing the flow in an axisymmetric aneurysm with steady laminar flow (Re<3000) showed the formation of an annular vortex for Reynolds number greater than 100 (5, 6). This vortex takes place in all the aneurysm and its center moved to the distal end when the Reynolds number increases. Formation of a second vortex might occur with high Re, 1750 and above (5). Pressure stayed mostly constant through the aneurysm with local peaks at the neck and the distal end where the flow reattached. Wall shear stress is close to zero along the aneurysm with a negative peak at the distal end due to the vortex center vicinity. The distal end waist induces a flow acceleration that sharply changes the wall shear stress sign. Such flow comportment is correlated to platelet deposition (6).
Pulsatile flow under axisymmetric models (2-5, 11, 12) all show the flow attachment during the systolic acceleration, the formation and growth of one or several vortices, depending on the flow intensity,

1722-6899/176-10$15.00/0

during the systolic deceleration, the displacement of vortex to the distal end during the early diastole and the holding or fragmentation of vortices during the late diastole. Pressure changes along the cardiac cycle but remains constant through the aneurysm. The wall shear stress remains close to zero within the aneurysm but peaks and sudden changes occur at the distal end due to the vortex and the aneurysm waist (4, 5, 11). Aneurysm asymmetry complexifies the flow description. The annular vortex is flattened on the less deformed side but follows the development pattern described before; secondary vortices are stronger in the diastolic phase (1-3). Like in the axisymetric case, pressure remains constant through the aneurysm. Wall shear stress concentration is still at the distal end. More precisely, it is maximum on the deformed side during late diastole and systolic acceleration, then maximum on the non deformed side during systolic deceleration (3). All previous models are developed with rigid wall. The latest models use actual geometry (1).

In the present study, blood flow behaviour in the three dimensional model of Abdominal Aortic Aneurysm is modeling numerically in laminar regime in a large range of Reynolds numbers (R_{mean}: 350 to 1400, R_{peak}:1640 to 2800). The aim of this project is the validation of real human AAA numerical simulation.

METHODS

The CT scan files used in this paper were taken from patients included in a research study that took place in three different hospitals (Notre Dame, St Luc, Hotel Dieu, Montréal, Québec, Canada) comparing surgical and endovascular treatment of AAA. This study was approved by the Institutional Review Board. In this study, patients signed an informed consent giving an access to their medical and imaging file. All radiological files were fully anonymized before post processing. The methodology is based on the geometry construction of human AAA, the generation of finite element domains and the simulation of blood flow.

Three-dimensional geometry reconstruction

The geometry is generated from a points cloud using computed tomography data, cutting the abdomen in the transversal plane. This AAA is 124 mm long, cut in 63 sections of 40 points, each section 2 mm apart. Inlet section has a mean diameter of 20 mm and the outlet section is more oval with 17 mm and 8 mm for the big and small axes. The biggest diameter is 45 mm.

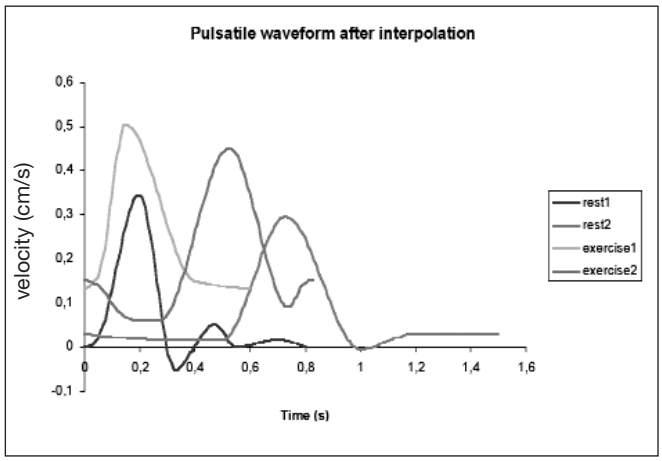

Fig. 1 - ***Rest 1 and exercise 1 are data from (13) and rest 2 and exercise 2 from (2).***

Blood flow and velocity waveforms

The flow is considered incompressible, homogeneous and Newtonian with rigid wall. The blood is simulated with a kinetic viscosity of 3.6×10^{-6} $m^2.s^{-1}$ and a density of ρ = 1050 $kg.m^3$. The boundaries conditions are: (i) no-slip at the walls, (ii) constant pressure (101×10^3 Pa) on the outflow section and (iii) homogeneous velocity profile at the entrance. A pipe five times longer than the entrance diameter gives a parabolic profile at the aneurysm entrance, and a pipe 110 mm long at the outlet section allows the flow to exit without influencing the flow in the aneurysm. The pulsate waveforms are obtained by cubic interpolation of points from (13) and (2) using Matlab software. There are two rests and two exercise patterns showed in Table I and Figure 1.

Computational modeling

Computational fluid dynamics (CFD) methods have been selected in this paper. The geometry of the aneurysm has first been transferred from CT data and further meshed using the interactive multi-purpose grid generation tool IGG™ developed by Numeca International (14). The governing Reynolds-averaged Navier-Stokes equations for blood flow have been solved using the flow solver Euranus integrated in Fine™ suite v6.2-1. The computational method is based on a second order cell-centered finite volume approach. The algorithm being based on the compressible form of the equations, a preconditioning method is applied for the

TABLE I - RANGE OF FLOW PARAMETERS

Activity level	**Rest 1**		**Rest 2**		**Exercise 1**		**Exercise 2**	
Hearth rate (beats.mn^{-1})	75		40		100		72.29	
Reynolds Number								
Remean	362.57		353.11		1388.00		1057.22	
Repeak	1916.66		1638.88		2800		2497.44	
Womersley Number	29.54		21.57		34.11		29.00	
	Time (s)	Velocity (cm.s^{-1})	Time (s)	Velocity (cm.s^{-1})	Time (s)	Velocity (cm.s^{-1})	Time (s)	Velocity (cm.s^{-1})
Plotting points for cubic interpolation (one pulsation)	0	0	0	3	0	13.3	0	15
	0.04	1.1	0.5	1.5	0.05	15.9	0.05	14
	0.2	34.5	0.73	29.5	0.15	50.4	0.125	8
	0.33	−5.3	1	−0.5	0.4	14.9	0.18	6.1
	0.4	0	1.2	3	0.6	13.3	0.275	6
	0.47	5.3	1.5	3			0.525	45
	0.55	0					0.74	9
	0.7	1.6					0.8	14.5
	0.8	0					0.83	15

simulation of incompressible flows so as to ensure an optimum convergence rate. In the present project, the preconditioning parameter β has been decreased to values as low as 30.

A central space discretization is additionally selected and a Jameson's type dissipative term is added to ensure stability. The integration of the discretized equations is carried out at each physical time step using a dual step procedure. The time associated to a heart pulse (≈ 0.8 sec depending of the pattern) has been split into physical time steps of $\Delta t = 0.01$ s. Pseudo-time integration towards each physical time step is carried out by a time-marching method using an explicit 4 steps Runge-Kutta scheme which is coupled with residual smoothing and multi-grid techniques. To ensure 4-orders of magnitude decrease in the residuals, a maximum of 1500 inner iterations is calculated at each physical time step and 5 heart pulse are computed in order to get rid of the numerical transient period. A typical calculation over one cycle of heart pulse took less than 1-day CPU on a single processor Pentium(R) 4.3 Ghz equipped with 1Go RAM. The hard disk space required for the storage of the corresponding mesh, project and solution files is of 11.7Go.

To ensure high convergence rates, a full multi-grid acceleration strategy based on 3 levels of grid is usually selected for all calculations. The solution is initiated on the coarsest grid level (referred to as level 222) and further interpolated on an intermediate grid (referred to as level 111) where a more complete convergence is reached. The solution is then transferred to the fine grid level (referred to as level 000) in order to reach complete convergence, confirmed by a decrease of minimum 4 orders of magnitude in residuals and stabilization of global performances of the propeller. Starting from the finest grid level, the coarse grid level is built by taking one grid node over 2 in each of the x-,y- and z- direction. As a consequence, a factor 8 (= 2^3) applies in the number of grid nodes going from the coarse to the fine grid. This technique is particularly efficient since it initiates fast convergence and furthermore enables to nicely check for grid dependency without the need to rework the mesh. In the present case and as a first approximation, the simulations have been conducted on the coarsest grid level 222. Potential mesh dependency effects have not been assessed.

The results have been extracted using the visualization and post-processing tool CFView™ v3.8-24 developed by Numeca. Specific macro-commands have been used for a fast and efficient treatment of the numerous data generated by a time-accurate simulation.

RESULTS AND DISCUSSION

Flow dynamics

The point cloud used to generate the model uses a Cartesian system and the z axis goes from the exit of the aneurysm to the entrance. We use the z axis

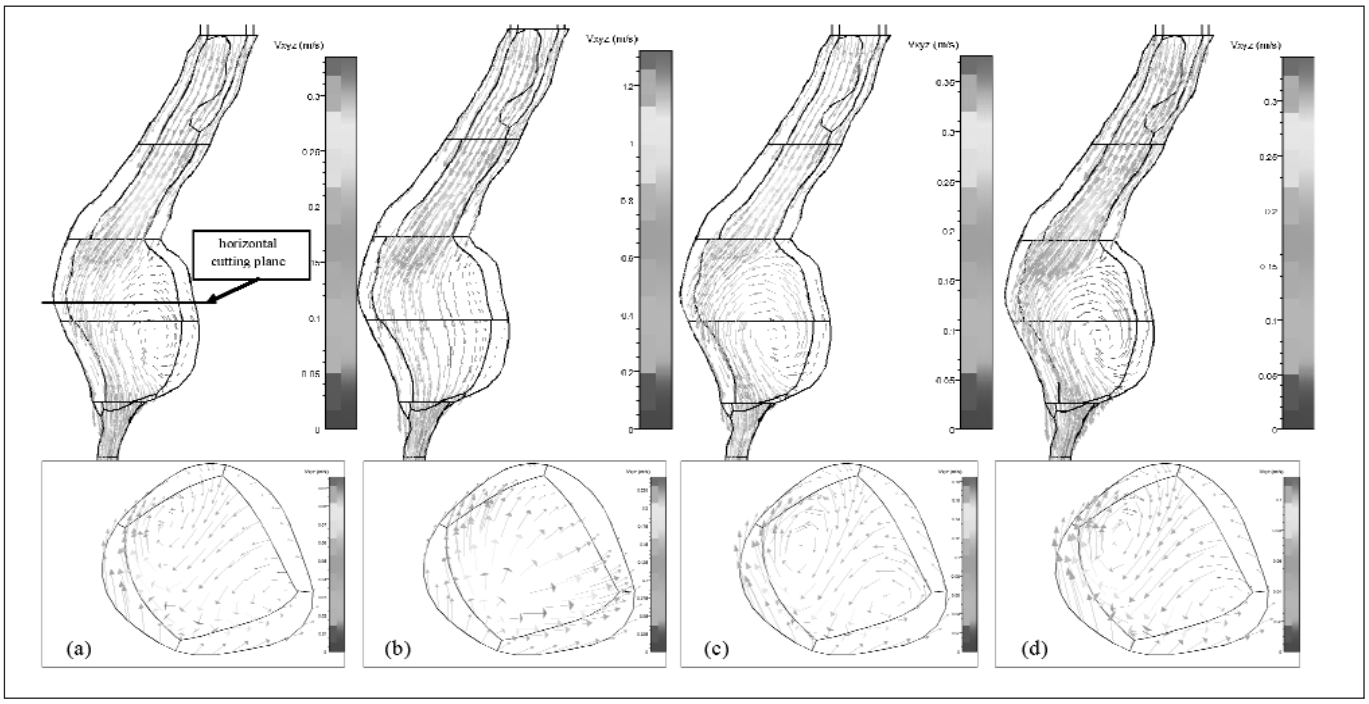

Fig. 2 - *Vertical cutting plane for exercise 1, at 0.01 s (a), 0.17 s (b), at 0.39 s (c), and 0.52 s (d).*

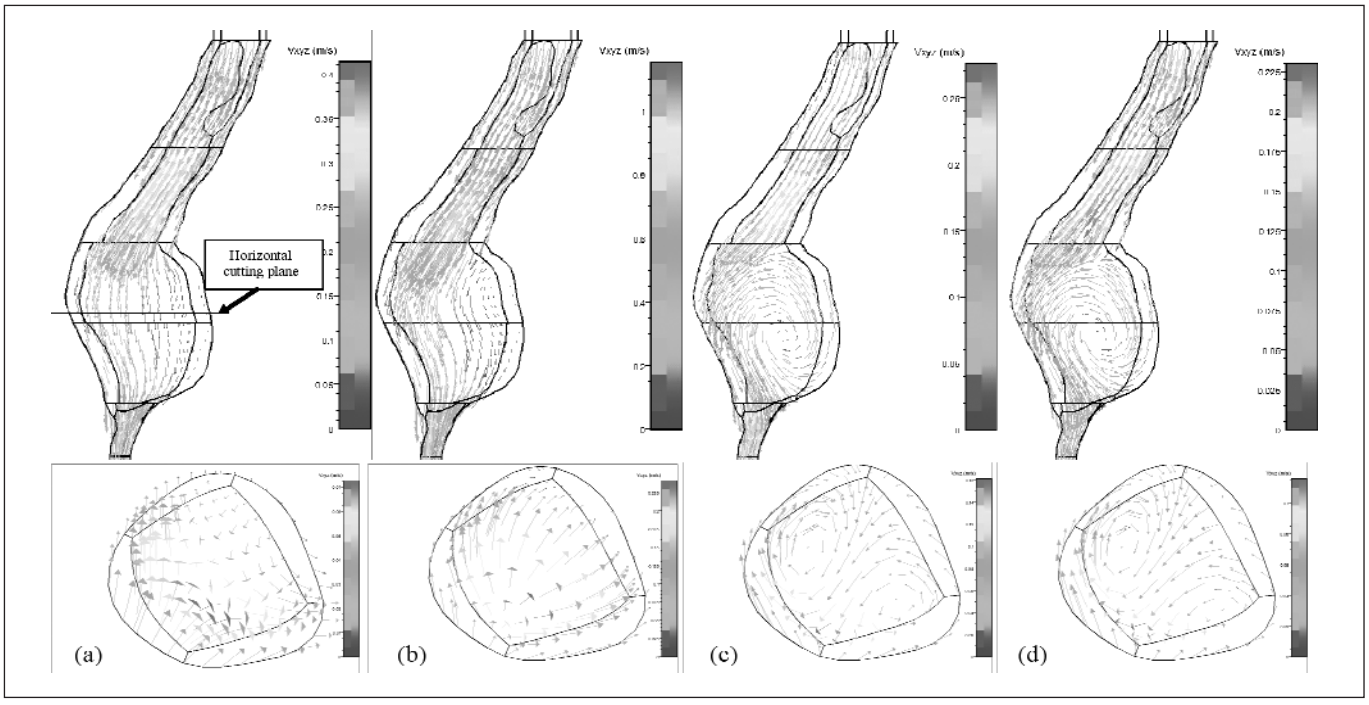

Fig. 3 - *Vertical cutting plane for exercise 2, at 0.39 s (a), 0.54 s (b), 0.74 s (c) and 0.82 s (d).*

to define the vertical. To follow the flow evolution, we use a vertical cutting plane which goes from the entrance of the aneurysm to the distal end and a transversal cutting plane.

Figure 2 and 3 show the flow evolution for the two exercise conditions. Evolutions are quite similar and can be qualitatively described in the same way. At the end of the diastole, beginning of the systole (0.01 s for exercise 1 and 0.39 s for exercise 2) the flow is regular at the top of the aneurysm and in the

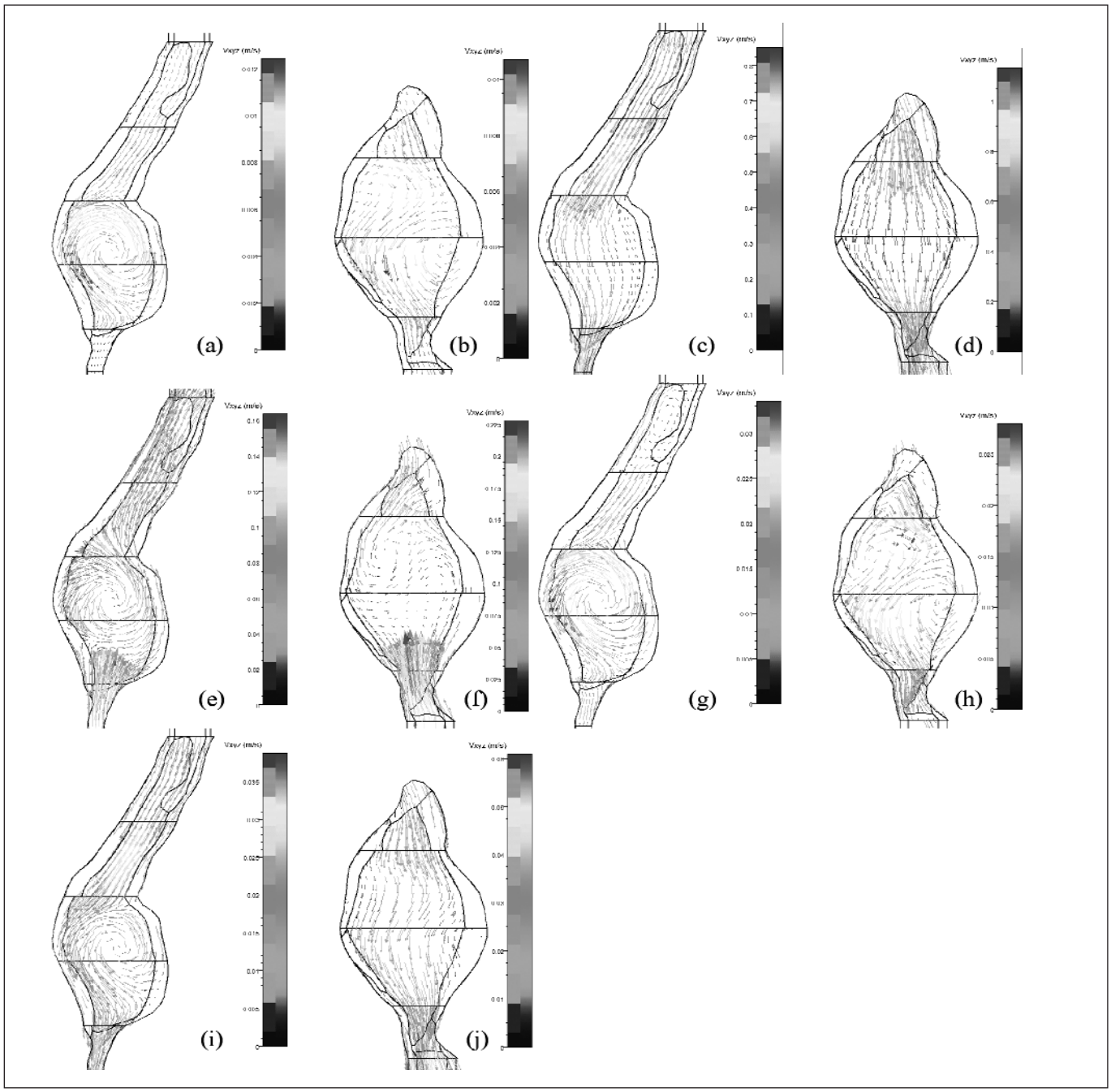

Fig. 4 - ***Rest 1: t = 0.02 s (a),(b); t = 0.22 s (c),(d); t = 0.33 s (e),(f); t = 0.54 s (g),(h); t = 0.71 s (i),(j).***

less deformed part. A vortex, seen in the vertical plane, takes place in the deformed part with secondary rotations in the horizontal plane. During the systolic acceleration (from 0.01 s to 0.17 s for exercise 1 and from 0.39 s to 0.54 s for exercise 2), the vortices are pushed out and the flow is regular through the entire artery. Just after the systolic peak (0.17 s for exercise 1 and 0.54 s for exercise 2), a vortex starts at the top of the deformed part of the artery. It grows during the systolic deceleration (from 0.17 s to 0.39 s for exercise 1 and from 0.54 s to 0.74 s for exercise 2) and moved toward the distal end, creating secondary horizontal vortices. During the diastole (from 0.39 to 0.52 s for exercise 1 and from 0.74 s to 0.39 s of the next cycle for exercise 2), vortices remain stable in shape and intensity.

Figure 4 shows the flow during the first resting condition. To complete the visualisation of the flow, we use a second vertical cutting plane instead of a

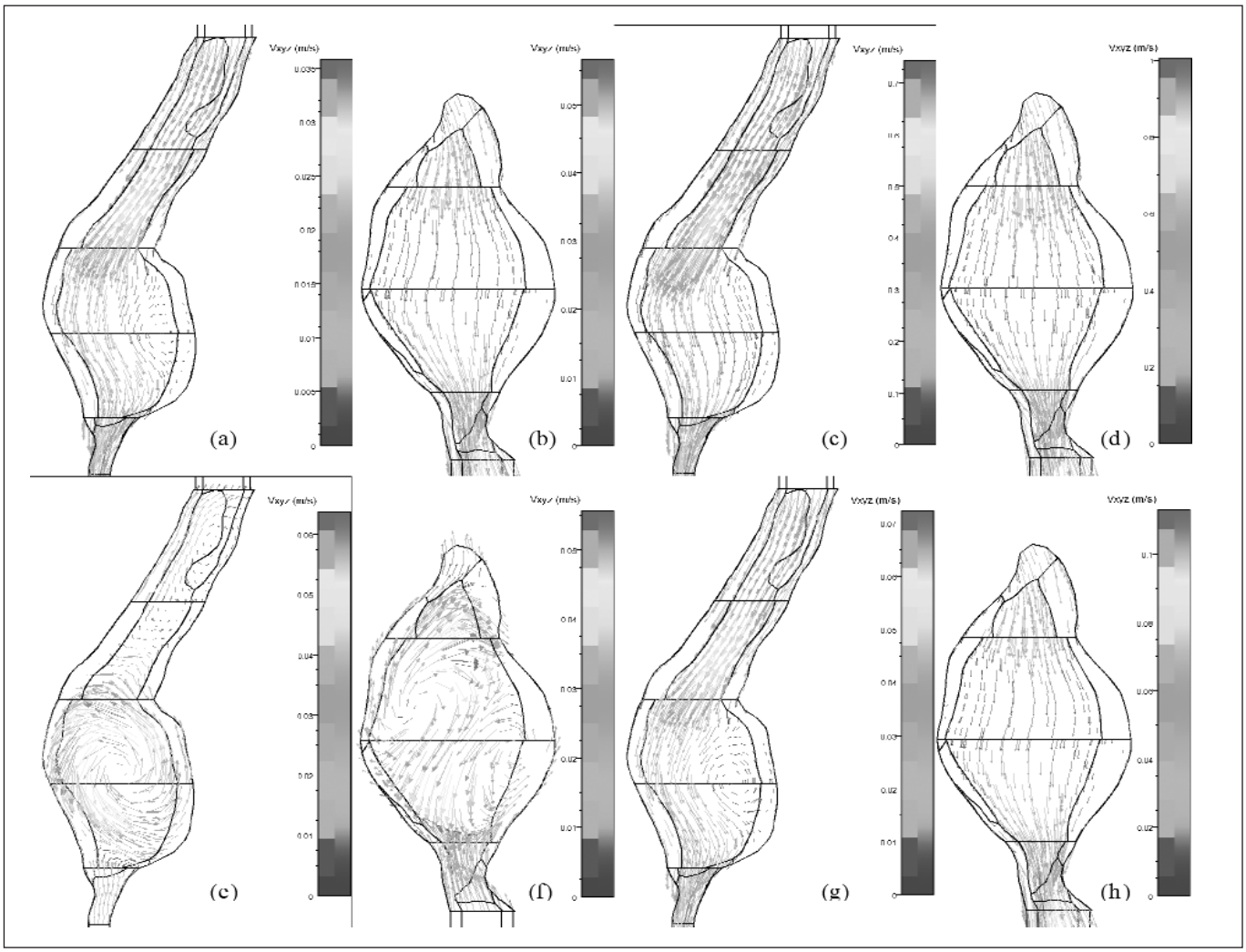

Fig. 5 - ***Rest 2: t = 0.50 s (a),(b); t = 0.75 s (c),(d); t = 1s (e),(f); t = 1.45 s (g),(h).***

transversal cutting plane, turned 90 degrees from the previous vertical plane. At t = 0.02 s (Fig. 4 a, b), end of the diastole, a vortex takes place in all the aneurysm and secondary rotations are visible in the second cutting plane. During the systolic acceleration (t = 0.02 s, Fig. 4 a, b, to 0.22 s, Fig. 4 c, d) all vortices are pushed out of the aneurysm and the flow reattached on the wall. Just after the systolic peak, a vortex appears in the aneurysm top and grows during all the systolic deceleration (t = 0.22 s, Fig. 4 c, d, to 0.33 s, Fig. 4 e, f). At t = 0.33 s (Fig. 4 e, f), the flow velocity reversed itself inducing secondary vortices in the aneurysm. This kind of oscillations of the velocity appear two times during the diastole, t = 0.54 s (Fig. 4 g, h) and t = 0.02 s (Fig. 4 a, b) of the next beat, but are less powerful and provoked smaller reversed flow.

Figure 5 shows the second resting condition flow. At the systolic end, t = 0.50 s (Fig. 5 a, b), a small vortex takes place in the middle of the aneurysm, and no secondary vortices are visible. The systolic phase follows the pattern described for the other flow conditions, i.e flow reattachment during the acceleration, vortex formation and grow during systolic deceleration. At the systole end, diastolic beginning (t = 1 s, Fig. 5 e, f), a small reverse flow occur, inducing secondary vortices. All along the diastole, t = 1 s (Fig. 5 e, f) to t = 0.50 s (Fig. 5 a, b) of the next beat, the flow and the aneurysm remain stable and small, as shown in the Figure 5 g and h.

Wall static pressure

During the cardiac cycle, for each cardiac waveform, spatial pressure change is small along the aneurysm as shown in Figure 2. That result agree with (1, 15) for a three dimensional asymmetric AAA model. Generally, the variation of pressure fol-

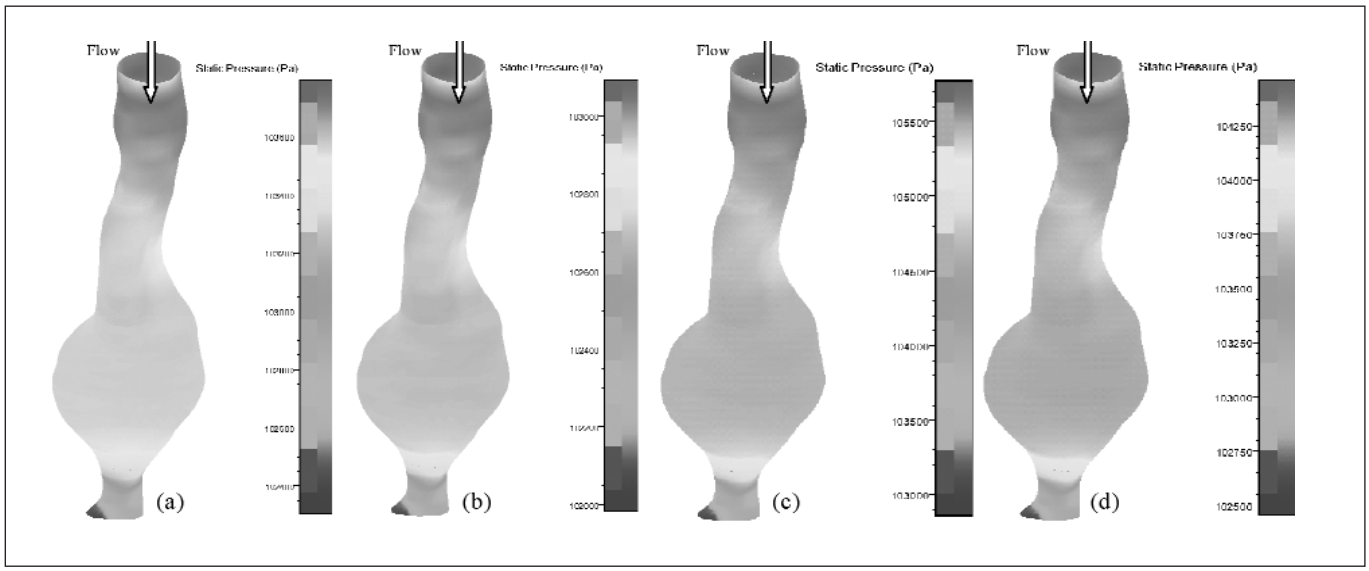

Fig. 6 - ***Wall static pressure distribution for each pulsate wave before the diastolic peak, rest 1 (a), rest 2 (b), exercise 1 (c), exercise 2 (d).***

lows the pattern imposed by the waveform from the inlet and pressure decrease slowly from the proximal end to the distal end, except during the diastolic end and systolic beginning of the rest waveform where the negative velocity imposed induces a pressure at the distal end higher than at the proximal end (Fig. 3).

CONCLUSIONS

Using different pulsate waveforms, we have simulated the flow within an actual aneurysm with rigid wall and Newtonian blood. The flow description for each waveform qualitatively matches to (1, 15) description according to the following steps.
Systolic acceleration: all residual vortices are pushed out of the aneurysm and the flow reattach to the wall.
Systolic deceleration: separation of the flow on the proximal of the most deformed part of the aneurysm, the just created vortex grows and moves downward.
Diastole: secondary vortices might appear depending on the waveform imposed, the principal vortex takes place in all the deformed part and weaken or sustain itself depending, once again, on the waveform imposed.
Our description of the last step differs from Finol's because of the different conditions imposed: on our resting waveform, we have oscillations around zero during the diastole and on our exercise waveform the velocity maintains itself above zero.
As for the pressure, results agree with the literature (2, 4, 11).
Perspectives: shear stress has not been discussed and it is the next step of the model improvement. Consideration of shear stress is very important to understand the physiologic reaction, the platelet deposition (6) and the formation of a thrombus. Once this step is complete, we will refine our model to reduce the time of calculation and use less interpolation. Long-term perspective is to develop fluid/structure interaction (CFD) models with actual geometry and introduce porous tubes in the aneurysm to simulate stents.

ACKNOWLEDGMENTS

Vincent Bouffioux (Numeca Inc. Belgium) provided technical support with the finite element software.
L'Hocine Yahia gived us acces to his laboratory and gave us his help.
Funding for this work was provided in part from the FRSQ, FCI and Valorisation-Recherche Québec (group grant # 2200-094).

Address for correspondence:
Kaouthar Saïdane, PhD
Biomedical Engineering Institute
Ecole Polytechnique de Montréal
Succ. Centre Ville, C. P. 6079
Montréal, QC, H3C 3A7 - Canada
Kaouthar.saidane@polymtl.ca

REFERENCES

1. Finol EA, Amon CH. Flow dynamics in anatomical models of abdominal aortic aneurysms: computational analysis of pulsatile flow. Acta Cient Venez 2003; 54: 43-9.
2. Egelhoff CJ, Budwig RS, Elger DF, et al. Model studies of the flow in abdominal aortic aneurysms during resting and exercise conditions. J Biomech 1999; 32: 1319-29.
3. Yip TH, Yu SC. Cyclic flow characteristics in an idealized asymmetric abdominal aortic aneurysm model. Proc Inst Mech Eng [H] 2003; 217: 27-39.
4. Finol EA, Amon CH. Flow-induced wall shear stress in abdominal aortic aneurysms: Part II–pulsatile flow hemodynamics. Comput Methods Biomech Biomed Engin 2002; 5: 319-28.
5. Finol EA, Amon CH. Flow-induced wall shear stress in abdominal aortic aneurysms: Part I–steady flow hemodynamics. Comput Methods Biomech Biomed Engin 2002; 5: 309-18.
6. Bluestein D, Niu L, Schoephoerster RT, et al. Steady flow in an aneurysm model: correlation between fluid dynamics and blood platelet deposition. J Biomech Eng 1996; 118: 280-6.
7. Dobrin PD. Physilogy and pathophysiology of blood vessels. In: Sidawy AN, Sumpio BE, DePalma RG, eds. The Basic Science of Vascular Disease. New York: Futura, 1997; 69-105.
8. Hsiang YN, Turnbull RG, Nicholls SC, et al. Predicting death from ruptured abdominal aortic aneurysms. Am J Surg 2001; 181: 30-5.
9. Inzoli F, Boschetti F, Zappa M, et al. Biomechanical factors in abdominal aortic aneurysm rupture. Eur J Vasc Surg 1993; 7: 667-74.
10. Vorp DA, Raghavan ML, Webster MW. Mechanical wall stress in abdominal aortic aneurysm: influence of diameter and asymmetry. J Vasc Surg 1998; 27: 632-9.
11. Finol EA, Amon CH: Blood flow in abdominal aortic aneurysms: pulsatile flow hemodynamics. J Biomech Eng 2001; 123: 474-84.
12. Viswanath N, Rodkiewicz CM, Zajac S. On the abdominal aortic aneurysms: pulsatile state considerations. Med Eng Phys 1997; 19: 343-51.
13. Cheng CP, Herfkens RJ, Taylor CA. Comparison of abdominal aortic hemodynamics between men and women at rest and during lower limb exercise. J Vasc Surg 2003; 37: 118-23.
14. Numeca International. IGG tm User manual 4.9-a. 2004.
15. Finol EA, Keyhani K, Amon CH. The effect of asymmetry in abdominal aortic aneurysms under physiologically realistic pulsatile flow conditions. J Biomech Eng 2003; 125: 207-17.